Received October 1996
Revised January 1997

Transient flow of homogeneous gas-liquid mixtures in pipelines

Ezzeddine Hadj-Taieb
Department of Mechanical Engineering, ENIS, Sfax Tunisia, and
Taieb Lili
Physical Department of Sciences Faculty, Tunis, Tunisia

1. Introduction

Since the beginning of the century, numerous theoretical and experimental studies on transients flow in piping systems have been investigated. From practical and industrial points of view, the interest has been focused on the prediction of the pressure fluctuations provoked by the so-called water-hammer phenomenon in the name sufficiently suggestive of possible damage caused to the pipelines and hydraulic components.

The circumstances where this pressure fluctuation appears are numerous, following voluntary disturbances (rapid valve closure) or accidental disturbances (sudden pump failure, pipelines rupture…).

Besides the history of the forced hydroelectric factory pipelines, which was at the origin of the development of many computation methods, we also mention, the water supply network, the irrigation pipeline systems, the petroleum pipelines and the natural gas-piping systems.

For a long time the classical theory of the transient flow has considered only single-phase flow of pure liquid, with constant compressibility, or highly deformable gas. Moreover, the pipe is assumed to behave linearly elastically with constant mechanical and geometrical properties and without inertia in radial and axial directions.

In gas dynamics the elastic properties of the pipelines are usually neglected and the acoustic velocity is a function of the pressure. For liquid, the elasticity and geometric characteristics of the pipe wall are generally incorporated in the pressure wave speed. The value of the wave speed, regarded as constant, is hence reduced from its value in the liquid.

It is known however, that industrial liquid and particularly water contains a small amount of free or dissolved gaseous phase. Consequently in many circumstances, such as in nuclear and geothermal power plants, in petroleum industries and in sewage pipelines, the two-phase transient flow involves fluid mixtures of different states, liquid and gaseous. The mixture may already exist in the steady state flow, as in sewage, or from the release of the gaseous phase when the fluid pressure is reduced to the saturation pressure of the dissolved gas.

International Journal of Numerical Methods for Heat & Fluid Flow
Vol. 8 No. 3, 1998, pp. 350–368.

It is well known[1,2] that the presence of small amounts of free gas in liquid reduces considerably the pressure wave speed in the mixture from that in the pure liquid itself. As the gas-liquid mixture is compressible the wave propagation velocity varies with the pressure and the system of equations describing the transient two-phase flow is non-linear. The study is then more complex and difficult than in pure liquid flow. The complexity arises when computing the wave front where some phenomena, e.g. the expansion waves spreading, the compression waves steepening and the shock wave inception may manifest[3].

Martin *et al.*[4,5] have developed a mathematical model constituting three differential equations representing the two-phase transient flow. By question of facility, finite difference Lax-Wendroff scheme was employed and preferred over the method of characteristics. They concluded that, for greater void fraction as in the slug flow the pressure surges may be adequately predicted by the homogeneous model.

Chaudry *et al.*[6] treated the gas liquid mixture as a pseudo-fluid when the void fraction was small. They used two second order explicit finite difference techniques coupled with the characteristic equations at the pipe boundaries. The problem of the shock wave simulation has not been examined.

An interesting study on propagation of pressure waves in vapour-liquid mixtures has been investigated by Mori *et al.*[7]. They have examined the pipe's elasticity effect on the velocity propagation of the pressure waves by considering void fraction change in relation to the pressure rise. The analytical results are compared to experimental data of shock waves in vertical tube.

Most of the above-mentioned investigations have modelled the homogeneous two-phase transient flow by using the void fraction which varies with the pressure.

In this study we re-examine this problem and present simplified and reliable mathematical models for describing transient in homogeneous two-phase flow by taking into account the pipe elasticity effect on the pressure wave propagation, whatever the quantity of free gas may be. Instead of the void fraction, the developed models use the gas-fluid mass ratio, or the quality as called by Pascal[8]. The quality is assumed to be constant and not dependent on the pressure. This assumption has the advantage that it reduces the number of the equation formulations and, later on, facilitates the numerical resolution. A conservative finite difference scheme is used in computational pressure evolution at different equidistant sections of the pipe. First we deal with the so-called rigid model where the pipe elasticity and the liquid compressibility are neglected. Some hypothetical examples are analysed to give judgement on the validity of this model and the limits of its applications. By including the liquid compressibility and the pipe elasticity the quasi-rigid model is developed. The numerical results obtained by the quasi-rigid model are compared with experimental results obtained in a laboratory.

2. Assumption

In addition to the habitual assumptions of plane flow, the following hypothesis should also be stated:

- The flow is supposed to be one dimensional.
- The wall shear stress is defined by the steady-state Darcy-Weisbach formula depending on the friction factor (Evangelesti *et al.*[9]).
- The slip velocity of gas bubbles relative to the liquid velocity is neglected (Kranenburg[10]). So the number of bubbles per unit fluid volume may be assumed to be constant and then the quality may also be considered as constant.
- The mixture is assumed to be made of small gas bubbles uniformly distributed in the liquid.

3. Mathematical formulation

3.1 Pipe elastic behaviour

The pipe conveying fluid at the pressure p, is assumed to be cylindrical of circular cross section A and pipe wall thickness e. In the case of quasi-rigid pipes (metal, concrete …), where the deformations are small, the elastic pipe wall behaviour is given by the well known simplified relationship

$$\frac{dA}{A\sqrt{A}} = \frac{2c}{Ee\sqrt{\pi}}\,dp \tag{1}$$

We may express the pipe section area in terms of the average absolute pressure, i.e.

$$A = A_0\left(1 - \frac{D_0 c}{2Ee}(p - p_0)\right)^{-2} \tag{2}$$

where E is Young's modulus for the pipe material, c is the pipe constraint factor and D is the circle pipe diameter such as $D = \sqrt{2}\,A/\pi$. 0 is a subscript referring to the initial conditions.

When the effect of the pipe elasticity may be neglected as in the case of the perfectly rigid pipes ($E \approx \infty$) the equation (2) is simplified to:

$$A = A_0 = Cte \tag{3}$$

3.2 Two-phase mixture density

The fluid mixture is made of liquid containing gas bubbles uniformly distributed and with evolution assumed to be polytropic:

$$\frac{p}{\rho_g^n} = \frac{p_0}{\rho_{g_0}^n} = Cte \tag{4}$$

If $M = M_l + M_g$ is the total mass of the fluid element with total volume $\partial = \partial_l + \partial_g$, then the density of the mixed fluid, ρ may be defined by

$$\frac{1}{\rho} = \frac{\vartheta}{M} = \frac{\vartheta_g + \vartheta_l}{M} = \frac{M_g}{M}\frac{\vartheta_g}{M_g} + \frac{M_l}{M}\frac{\vartheta_l}{M_l} \tag{5}$$

By noting $\theta = \frac{Mg}{M}$, the gas-fluid mass ratio or the quality, ρ may be expressed in terms of the two components densities as follows:

$$\frac{1}{\rho} = \frac{\theta}{\rho_g} + \frac{1-\theta}{\rho_l} \tag{6}$$

By using the bulk liquid modulus of elasticity K_l defined by:

$$\frac{1}{\rho_l}\frac{d\rho_l}{dp} = \frac{1}{K_l} \tag{7}$$

the liquid density may ρ_l be written:

$$\rho_l = \rho_{l_0} e^{(p - p_0)/K_l} \tag{8}$$

and it follows from (4) and (6) that

$$\rho = \left[\frac{\theta}{\rho_{g_0}}\left(\frac{p_0}{p}\right)^{1/n} + \frac{1-\theta}{\rho_{l_0}} e^{(p_0 - p)/K_l}\right]^{-1} \tag{9}$$

If the liquid is considered incompressible, i.e. $K_l \approx \infty$, equation (9) becomes:

$$\rho = \left[\frac{\theta}{\rho_{g_0}}\left(\frac{p_0}{p}\right)^{1/n} + \frac{1-\theta}{\rho_{l_0}}\right]^{-1} \tag{10}$$

3.3 Motion equations

The equations which describe transient one-dimensional flow can be adapted from the analytical model developed by Streeter and Wylie[11]. Applying the law of conservation of mass and momentum, to an element of fluid between two sections x and $x + dx$ of the pipe, yields the following equations of continuity and motion:

$$\frac{\partial \rho A}{\partial t} + \frac{\partial \rho A V}{\partial x} = 0 \tag{11}$$

$$\frac{\partial V}{\partial t} + V\frac{\partial V}{\partial x} + \frac{1}{\rho}\frac{\partial p}{\partial x} = gI - \frac{\lambda}{2D}V|V| \tag{12}$$

where V is the fluid velocity, I the slope of the pipe, λ is the coefficient of friction, t is the time and x is the distance along the pipe.

The continuity equation (11) is in the so-called conservative form. Equation of motion (12) can also be formulated in such form, that is:

$$\frac{\partial V}{\partial t} + \frac{\partial}{\partial x}\left[\frac{V^2}{2} + G(p)\right] = gI - \frac{\lambda}{2D}V|V| \tag{13}$$

where $G(p) = \int dp/\rho$.

3.4 Rigid model

Here the liquid compressibility and the pipe elasticity are neglected against the gas compressibility. Using pipe section area and fluid density expressions (3) and (10), we have:

$$G(p) = \left[\frac{n}{n-1}\frac{\theta}{\rho_{g_0}}\left(\frac{p_0}{p}\right)^{1/n} - \frac{(1-\theta)}{\rho_{l_0}}\right]p \tag{14}$$

and

$$A = A_0 = Cte \text{ and } \rho = \left[\frac{\theta}{\rho_{g_0}}\left(\frac{p_0}{p}\right)^{1/n} + \frac{1-\theta}{\rho_{l_0}}\right]^{-1} \tag{15}$$

3.5 Quasi-rigid model

By taking into account the pipe elasticity and liquid compressibility, the cross section area A is expressed by equation (2) and the fluid density by equation (9). The quasi rigid model is governed by equations (11) and (13) where:

$$G(p) = \frac{n}{n-1}\frac{\theta}{\rho_{g_0}}p\left(\frac{p_0}{p}\right)^{1/n} - \frac{K_l(1-\theta)}{\rho_{l_0}}e^{(p_0 - p)/K_l} \tag{16}$$

and

$$A = A_0\left(1 - \frac{D_0 c}{2Ee}(p - p_0)\right)^{-2} \text{ and } \rho = \left[\frac{\theta}{\rho_{g_0}}\left(\frac{p_0}{p}\right)^{1/n} + \frac{1-\theta}{\rho_{l_0}}e^{(p_0 - p)/K_l}\right]^{-1} \tag{17}$$

4. Numerical solution

The continuity and motion equations (11) and (13) constitute a non-linear hyperbolic system which could in principle be solved using the method of integration along characteristics[4]. However this method presents considerable difficulties because of the change of the wave celerity with pressure. For extreme pressure fluctuations shock waves may be formed by the steepening of compression waves.

Written in a conservation form the system of continuity and motion equations (11) and (13) can be solved by the two-step finite difference S_{β}^{α} scheme. This method is preferred over the characteristics method for many reasons[12].

First, the equations of continuity and motion formulated in conservation form are arranged in function of the two dependent variables V and p as follows:

$$\frac{\partial F_1(p)}{\partial t} + \frac{\partial F_2(p,V)}{\partial x} = 0$$
$$\frac{\partial V}{\partial t} + \frac{\partial F_3(p,V)}{\partial x} = F_4(p,V) \qquad (18)$$

where

$$F_1(p) = \rho(p)A(p) \qquad F_2(p,V) = F_1(p)V$$
$$F_3(p,V) = V^2/2 + G(p) \qquad F_4(p,V) = gI - (\lambda/4)\sqrt{\pi/A(p)}V|V| \qquad (19)$$

Over the entire (x, t) diagram, a grid is superimposed, the meshes of which have generally constant sizes $(\Delta x, \Delta t)$, see Figure 1. Following the techniques described by Richtmeyer and Morton[13] and Peyret and Taylor[14], the two-step S_{β}^{α} scheme used on conservative equation (18) is as follows:

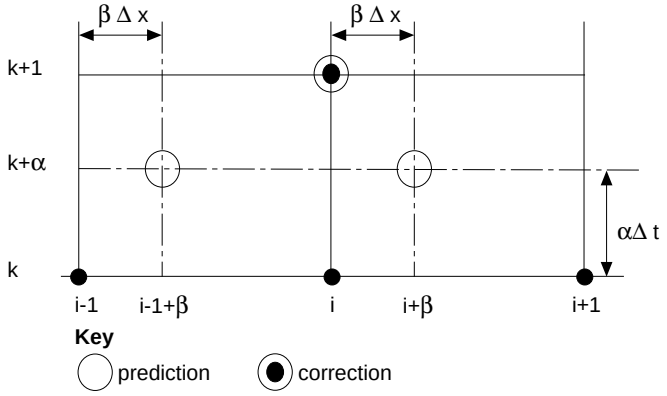

Figure 1. Finite differences scheme

First step of prediction (instant $(k + \alpha)\Delta t$):

$$(F_1)_{i+\beta}^{k+\alpha} = (1-\beta)(F_1)_i^k + \beta\,(F_1)_{i+1}^k - \alpha\sigma\left[(F_2)_{i+1}^k - (F_2)_i^k\right]$$
$$(V)_{i+\beta}^{k+\alpha} = (1-\beta)(V)_i^k + \beta\,(V)_{i+1}^k - \alpha\sigma\left[(F_3)_{i+1}^k - (F_3)_i^k\right] + \frac{\Delta t}{2}\left[(F_4)_{i+1}^k + (F_4)_i^k\right] \quad (20)$$

Second step of correction (instant $(k + 1)\Delta t$):

$$(F_1)_i^{k+1} = (F_1)_i^k - \frac{\sigma}{2\alpha}\left[(\alpha-\beta)(F_2)_{i+1}^k + (2\beta-1)(F_2)_i^k + (1-\alpha-\beta)(F_2)_{i-1}^k + (F_2)_{i+\beta}^{k+\alpha} - (F_2)_{i+\beta-1}^{k+\alpha}\right]$$
$$(V)_i^{k+1} = (V)_i^k - \frac{\sigma}{2\alpha}\left[(\alpha-\beta)(F_3)_{i+1}^k + (2\beta-1)(F_3)_i^k + (1-\alpha-\beta)(F_3)_{i-1}^k + (F_3)_{i+\beta}^{k+\alpha} - (F_3)_{i+\beta-1}^{k+\alpha}\right] + \Delta t\left[(F_4)_i^k\right] \quad (21)$$

In these equations $\sigma = \Delta t/\Delta x$ is the grid-mesh ratio and α, β two parameters of values generally satisfying the conditions $0 \le \alpha, \beta \le 1$. The S_β^α scheme is a three points explicit method accuracy. It can be shown that the requirement condition for stability is:

$$\sigma \le 1/(|V| + C) \quad (22)$$

where C is the pressure wave celerity given by[15]:

$$C = \left(\frac{\partial \rho}{\partial p} + \frac{\rho}{A}\frac{\partial A}{\partial p}\right)^{-1/2} \quad (23)$$

In the case of rigid wall conduit, the wave celerity C is simplified and has the following expression represented in Figure 2:

$$C = (\partial\rho/\partial p)^{-1/2} = \left(\theta n p_0/\rho_{g_0}\right)^{1/2}(p/p_0)^{(n-1)/2n}\left[1 + (1-\theta)\rho_{g_0}/\theta\rho_{l_0}\,(p/p_0)^{1/n}\right] \quad (24)$$

If the liquid compressibility and pipe wall elasticity are introduced, the celerity equation (23) can be written in the following way:

$$\frac{1}{C^2} = \frac{1}{C_0^2} + \frac{2c\sqrt{A_0/\pi}/(eE)}{1 + \left[c\sqrt{A_0/\pi}/(eE)\right](p_0 - p)}\,\frac{1}{\left[\theta/\left(\rho_{g_0}(p/p_0)^{1/n}\right) + (1-\theta)/\left(\rho_{l_0}e^{\left((p-p_0)/K_l\right)}\right)\right]} \quad (25)$$

where:

$$C_0^2 = \frac{\partial p}{\partial \rho} = \frac{\left[\theta/\left(\rho_{g_0}(p/p_0)^{1/n}\right) + (1-\theta)/\left(\rho_{l_0}e^{(p-p_0)/K_l}\right)\right]^2}{\theta/\left(n\rho_{g_0}p(p/p_0)^{1/n}\right) + (1-\theta)/\left(K_l\rho_{l_0}e^{(p-p_0)/K_l}\right)} \quad (26)$$

In this case, the wave celerity is shown in Figure 3 ($E = 2.10^{11}$) and in Figure 4 ($\theta = 10^{-6}$) as a function of the absolute pressure. Other data are the following:

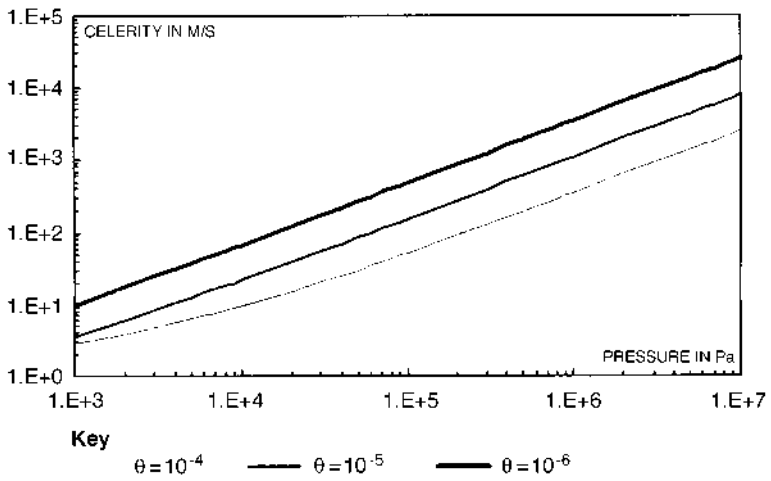

Figure 2.
Pressure wave celerity in rigid pipes

$K_1 = 2.10^9$ *Pa*, $D = 2m$, $e = 2cm$, $c = 0.9$, $\rho_{g_0} = 1.29$ Kg/m^3, $n = 1.4$, $p_0 = 10^5$ *Pa*, $\rho_{l_0} = 1{,}000$ Kg/m^3.

Computations carried out with the two-step S_{β}^{α} scheme showed that it yields satisfactory results. The oscillations in the front of the shock wave produced by extremely transient pressure fluctuations may be suppressed by increasing the value of σ just to the limit of the stability condition (22). Equation (21) of the numerical scheme described herein gives directly the value of the velocity V_I^{K+1}. Iterative method, such as the Newton-Raphson technique[16], is used to compute the pressure p_i^{k+1} from the calculated value of $[F1(p)]_i^{k+1}$

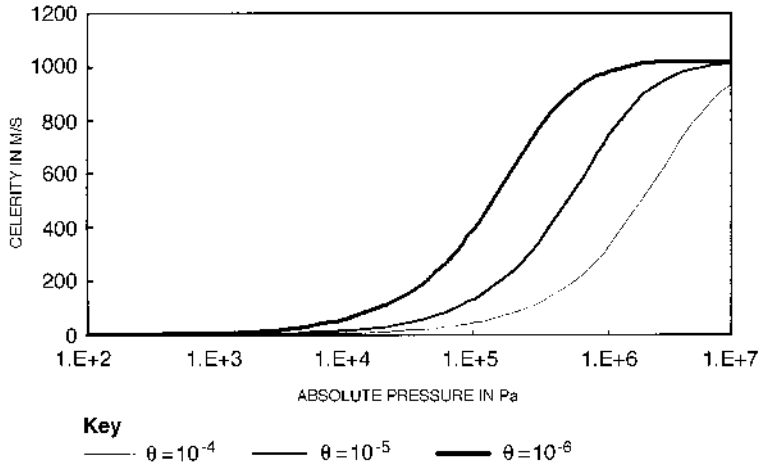

Figure 3.
Pressure wave celerity in quasi-rigid pipes

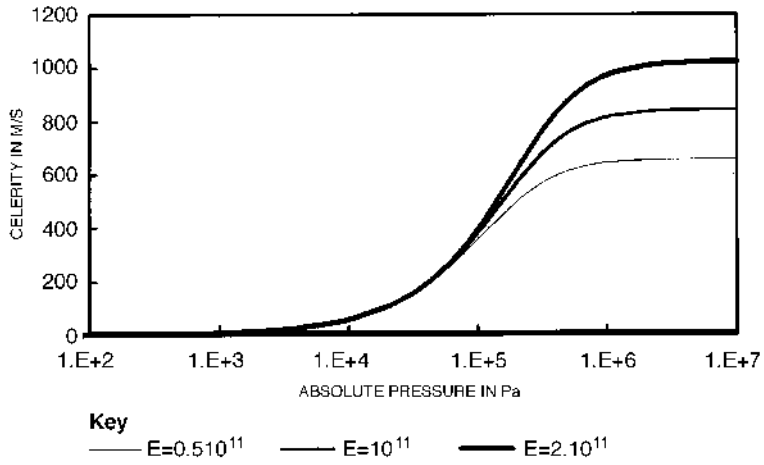

Figure 4.
Pressure wave celerity in quasi-rigid pipes

$$p_{m+1} = p_m - \frac{\rho(p_m)A(p_m) - F_1}{\frac{\partial(\rho A)}{\partial p}(p_m)} = p_m - \frac{\rho(p_m)A(p_m) - F_1}{\left[A\frac{\partial \rho}{\partial p} + \rho\frac{\partial A}{\partial p}\right](p_m)} = p_m - \frac{\rho(p_m) - F_1/A(p_m)}{\left[\frac{\partial \rho}{\partial p} + \frac{\rho}{A}\frac{\partial A}{\partial p}\right](p_m)} \quad (27)$$

By using the relation (23), the following iterative formula is obtained:

$$\begin{cases} \left(p_i^{k+1}\right)_0 = p_i^k \\ \left(p_i^{k+1}\right)_{m+1} = \left(p_i^{k+1}\right)_m - C^2\left[\left(p_i^{k+1}\right)_m\right]\left\{\rho\left[\left(p_i^{k+1}\right)_m\right] - \left[F_1(p)\right]_i^{k+1} \Big/ A\left[\left(p_i^{k+1}\right)_m\right]\right\} \end{cases} \quad (28)$$

which indicates that the wave speed takes place directly in the numerical scheme.

The values of the hydraulic parameters at time corresponding to $k = 0$, are given by the initial steady state conditions.

5. Computations and results

5.1 Rigid model applications

Example 1. Consider the hypothetical hydraulic system shown by Figure 5. The pipeline is of a length L = 20,000 m, a diameter $D_0 = 2m$, a pipe wall thickness e_0 = 2cm, an elasticity Young Modulus $E_0 = 2.10^{11}$ Pa and a constraint factor c = 0.9. The fluid properties are: ρ_{l_0} = 1,000 Kg/m_3, $p_0 = 10^5$ Pa, $\rho_{g_0} = 1.29$ Kg/m^3, n = 1.4, $K_l = 2.10^9$ Pa. The head pressure at the pump is H_0 = 100 m, the initial flow rate is Q_0 = 7,30 m^3/s and the friction factor is λ = 0.025.

Initial conditions. The steady state conditions ($p_0(x)$, $V_0(x)$) can be determined by computing the solution of the following system of ordinary differential equations:

$$dF_2(p,V)/dx = 0 \quad \text{and} \quad dF_3(p,V)/dx = F_4(p,V) \tag{29}$$

with the values for $x = 0$:

$$p_0(0) = \rho(p_0(0))gH_0 + p_0 \quad \text{and} \quad V_0(0) = 4Q_0/(\pi D_0^2) \tag{30}$$

The desired solution may be obtained by the Runge Kutta method[16]. The results are presented in Figure 6.

Boundary conditions. Transient flow is provoked by a rapid pump failure at $x = 0$, that is for $t > 0$: $V(0, t) = 0$. At the downstream end, $x = L$ and $t > 0$, the condition is given by the reservoir at fixed level: $p(L, t) = p0(L)$.

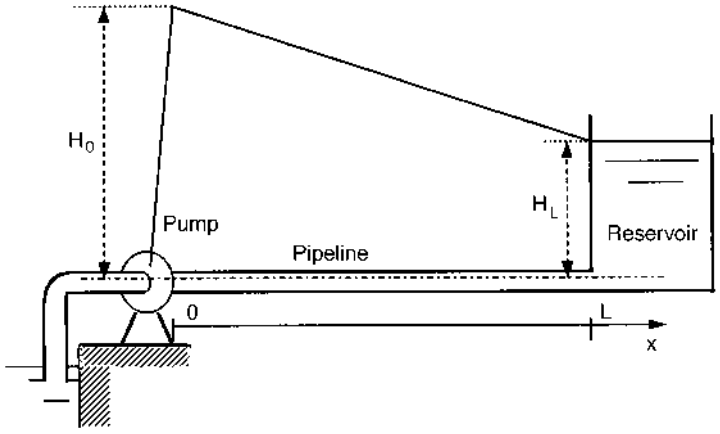

Figure 5.
Hydraulic system

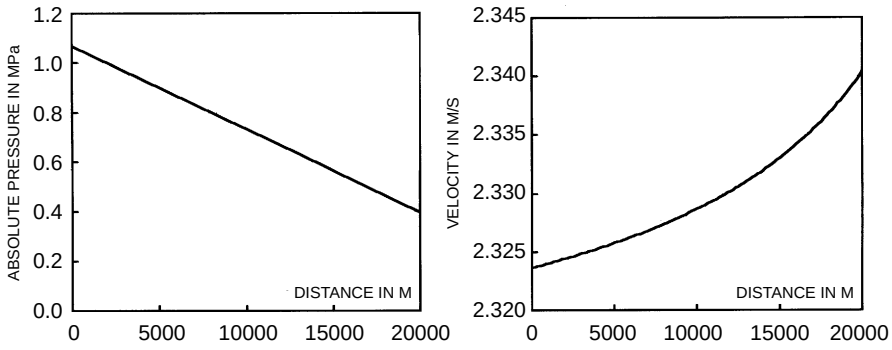

Figure 6.
Steady state conditions for $\theta = 10^{-4}$

Results and discussion. The S^{α}_{β} method was employed permitted to simulate correctly the pressure wave propagation. The pipe was divided into N equidistant sections in the x directions. The values of the hydraulic parameters at the pipe boundaries were simulated in the model without using characteristic equations but deduced directly from the numerical scheme equations (20,21).

The numerical results obtained for rigid model are shown in Figures 7-9. The respective used values of the quality are $\theta = 10^{-4}$, $\theta = 5.10^{-5}$, $\theta = 10^{-5}$, $\theta = 5.10^{-6}$, and $\theta = 10^{-6}$. Figure 7 shows, for $\theta = 10^{-5}$, $\theta = 5.10^{-5}$ and $\theta = 10^{-5}$, the computed pressure curves at some cross sections of the pipe ($x = 0$, $x = L/4$, $x = L/2$, $x = 3L/4$) obtained by the scheme S^1_0 with $N = 120$ and $\Delta t = L/[N^*(V_0(0) + C(p_0(0)))]$. It illustrates the phenomenon we are dealing with in the case of rigid pipe ($E = \infty$). After the sudden pump failure, a negative pressure wave travels along the steady state pressure gradient until it reaches the downstream end of the pipe. A region of depression is developed for some time depending on the value of θ. The positive reflected pressure wave travelling from the ends of the pipe causes a pressure rise. The pressure rise propagates in both directions and is reflected at the ends. The process repeats itself until the waves have dumped at the final steady state pressure.

In Figure 7, it is possible to see that the presence of a relatively great quantity of free gas smoothes the initial reflected suppression which nevertheless reaches the initial steady state pressure. This can be explained by the fact that for great values of θ, the fluid mixture becomes more compressible, which increases its capacity to absorb the pressure surges.

Figures 8 and 9 indicate that the velocity of the reflected compression wave at the upstream end was much larger compared with that of the incident wave, and the amplitude pressure after reflection was much larger compared with that before the reflected wave. It can also be noted that the obtained pressure amplitude and frequency evolve against the quality. The peak of the initial reflected pressure becomes very important for the low values of the quality; $\theta = 10^{-5}$ (Figure 7), $\theta = 5.10^{-6}$ (Figure 8), and $\theta = 10^{-6}$ (Figure 9). For the last two cases different values of the time increment Δt are used in computational pressure evolution (see Table I).

As pointed by Wiggert and Sundquist[17] it is difficult to cope numerically with a medium in which the wave speed is highly variable (see Figure 2). With the non constant time increment, the finite differences scheme has no fixed grid and the first pressure peaks (11MPa for $\theta = 10^{-6}$, and 2.3MPa for $\theta = 5.10^{-6}$) are captured with high accuracy.

It can be noted, however, that for these low values of the quality, the exactitude of the numerical results is considerably deteriorated. Indeed, the pressure amplitudes, which are very accentuated, are physically unreasonable and in contradiction with the classical water-hammer theory. This causes invalidation of the rigid model, that is, the assumption of rigid pipe and incompressible liquid should in no case be used for two-phase-flow with relatively low values of θ.

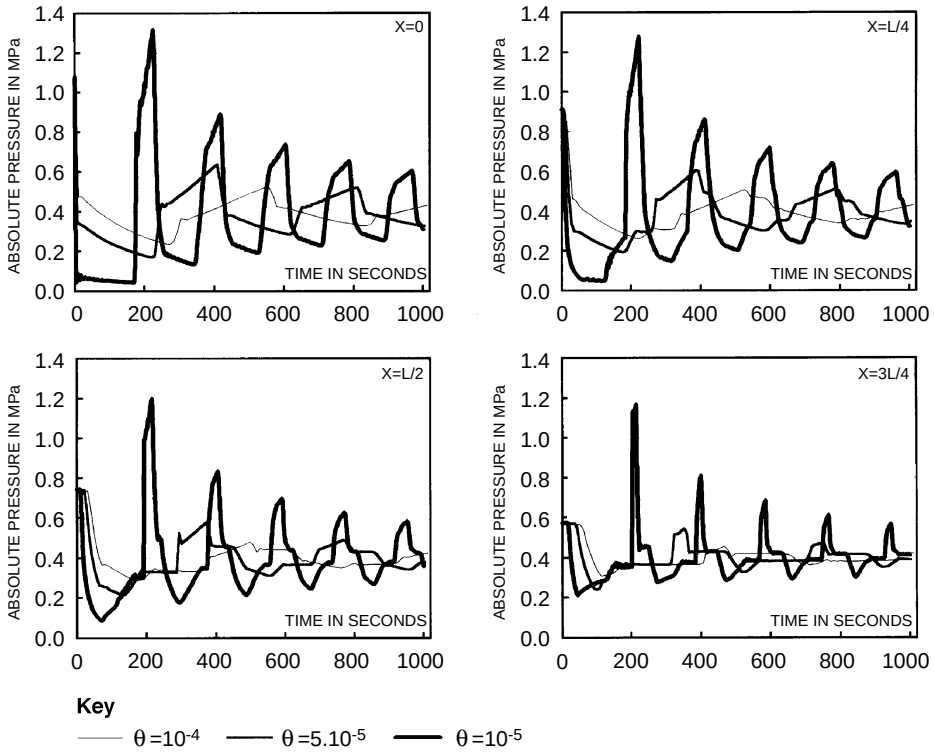

Figure 7.
Pressure curves for different values of θ

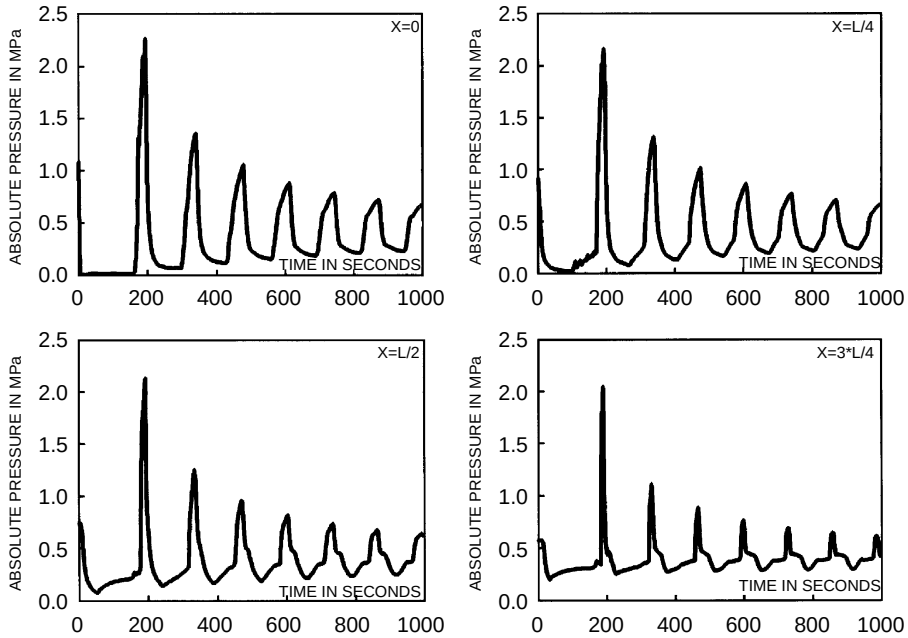

Figure 8.
Pressure curves for $\theta = 5.10^{-6}$

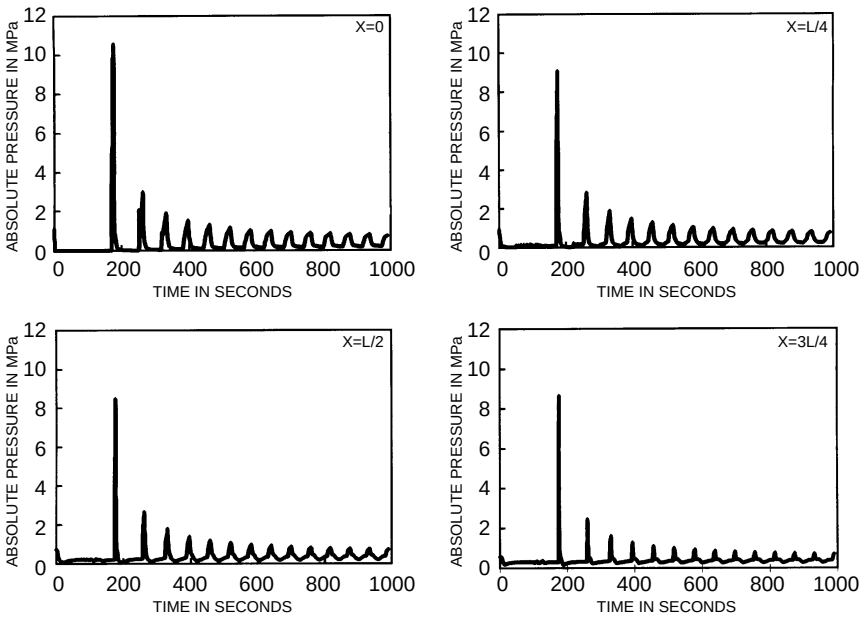

Figure 9.
Pressure curves for $\theta = 10^{-6}$

$\theta = 5.10^{-6}$	t (sec)	0	165.93	251.02	319.30	408.8		1,000.0	
N = 60	Δt (sec)	0.228	0.127	0.228	0.15	0.228			
	t (sec)	0	171.19	181.6	245.9	274.37		325.4	
$\theta = 10^{-6}$	Δt (sec)	0.1019	0.01	0.1019	0.032	0.1019			
N = 60	t (sec)		343.4	392.3	409.99	1,000.0			
	Δt (sec)	0.06	0.1019	0.08	0.085				

Table I.
Different values of the time increment

To verify the limits of the validity of the rigid model and the numerical scheme presented in the previous sections, two particular values of the mass concentration, $\theta \approx 1$ and $\theta \approx 0$, have been examined.

Example 2. We have considered the example studied by Esfandiari[18], concerning the dynamic of gas in a tube. The tube is closed at the upstream end and initially obtured by a diaphragm at the downstream end (see Figure 10). The dimensions of the tube are L = 1.515m and D = 25cm. Initially the tube contains air at the pressure $p_0(x) = 1.2310^5 Pa$ and the velocity $V_0(x) = 0m/s$. The

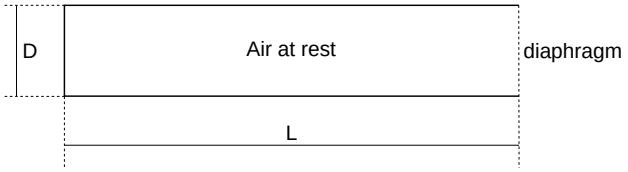

Figure 10.
Gas dynamic system

transient flow is produced by sudden rupture of the diaphragm at the extremity $x = L$. So the boundaries conditions are given by:

$$\begin{cases} p(L,t) = 10^5\, Pa \\ V(0,t) = 0 \end{cases}$$

For the value of $\theta = 1$ we have superposed in Figure 11 the pressure curves at $x = 0$, obtained by the rigid model based on the S_0^1 scheme and by the dynamic gas model computed by the characteristics method[18]. The agreement is satisfactory.

Example 3. Experimental validation has also been conducted by examining the classical water-hammer problem, corresponding to $\theta \approx 0$ (pure liquid), in a copper horizontal pipe connected at the upstream end to a constant level reservoir. The transient flow is generated by a quick closing solenoid valve situated at the downstream end of the pipe (see Figure 12). Additional data not included in Figure 12 are: $L = 35.7$m, $D_0 = 0.0196m$, $E = 0.910^{11}\, Pa$, $e = 0.001m$, $c = 0.9$ $p_0(0) = 0.263MPa$, $Q_0 = 0.000031\ m^3$/s.

The experimental results of the pressure surges are presented in Figure 13 and compared to the computed pressure obtained by the rigid model with $\theta = 10^{-7}$. The comparison indicates discrepancy between the numerical results and the experiment measurements. The unrealistic pressure spikes in the experimental curve are due to the recording system and the employed transducer's pressure.

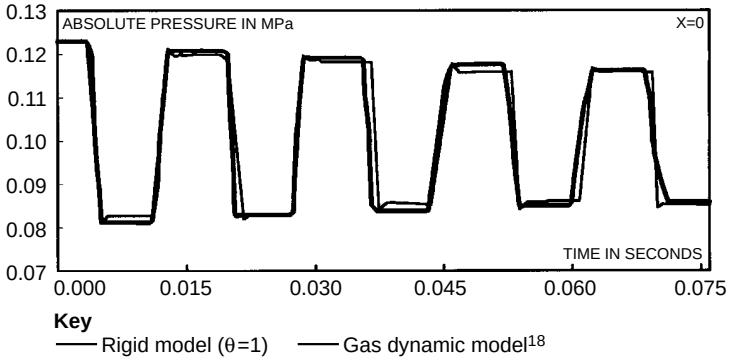

Figure 11.
Pressure evolution at the upstream end of the tube

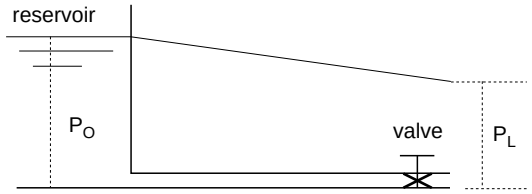

Figure 12.
Single pipeline with valve at the downstream end

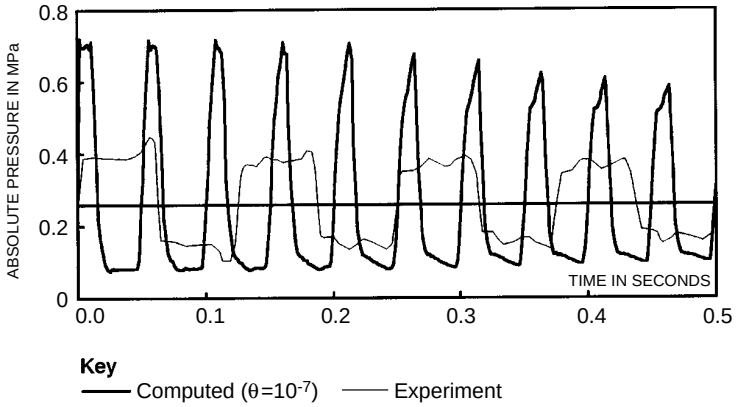

Figure 13.
Pressure evolution at the downstream end of the pipe

The finding is in accord with physical reasoning: in fact one would expect that the mixtures with smaller quality exhibit greater stiffness and therefore greater celerity, than the mixtures with greater quality.

We can conclude that the rigid model is reasonably accurate as far as the quality is important, but is incapable to investigate a two-phase transient with very low values of quality.

Quasi-rigid model applications

Experimental validation

To validate the concept of the quasi-rigid formulation, the previous experimental results of the example 3 on water-hammer have been reviewed. Figures 14 and 15 show the comparison with the numerical results from the quasi-rigid model with different values of θ and λ. The values of the wave celerity, are presented in Table II.

For the very low values of θ, especially for $\theta = 0$ (see Figure 15), the numerical curves approach better the experimental pressure recording. For

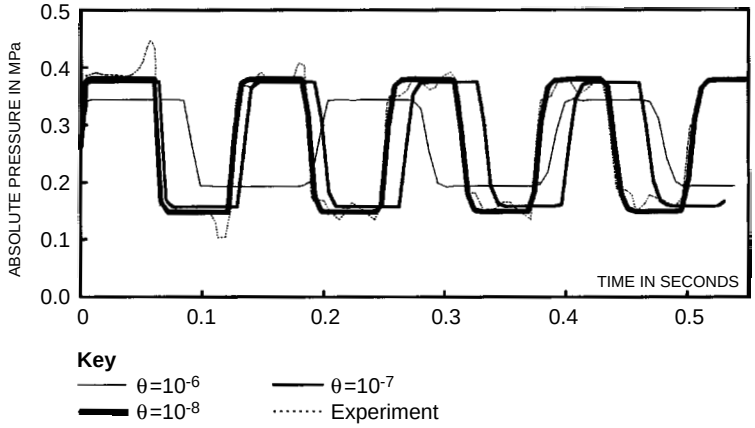

Figure 14.
Pressure evolution obtained by the quasi-rigid model

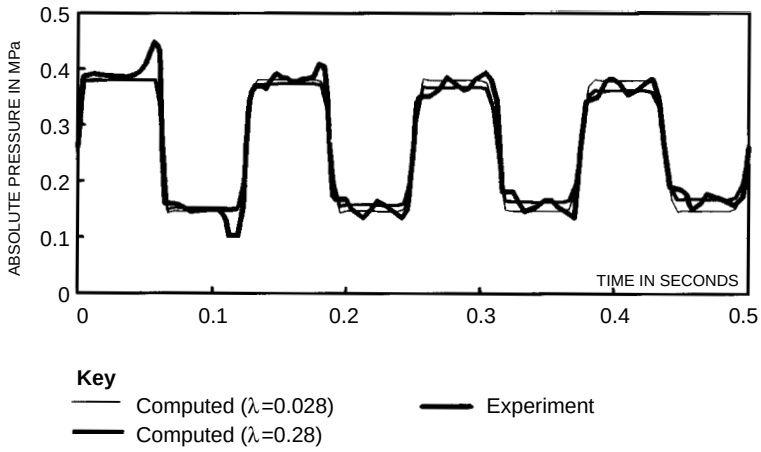

Figure 15. Pressure evolution obtained by the quasi-rigid model with $\theta = 0$

	Quasi-rigid model E = 0.9 10^{11}			Experiment
θ	10^{-6}	10^{-7}	10^{-8}	0
$C(p_0(0))$	740 m/s	1,071.5 m/s	1,135.5 m/s	1,143.4 m/s

Table II. Values of the wave celerity for different values of θ

these values, the timing of the positive and negative pressure waves obtained by the quasi-rigid model follows the experimental curve quite closely. However the predicted damping is less than that measured. It can be said that the quasi-rigid model produces results that compare better with the experiment than those from the rigid model.

Numerical validation

In order to test numerically the validity of the quasi-rigid model, the hydraulic system of the example one shown in Figure 5 has been reconsidered. The numerical model formulated was used to predict the performance of the pressure surges when taking into account the liquid compressibility and the pipe wall elasticity. Figure 16 shows the simulation results for $E = 2.10^{11}$ Pa, and for different values of the quality $\theta = 10^{-5}$, $\theta = 5.10^{-6}$ and $\theta = 10^{-6}$. For different values of Young modulus: $E = 0.510^{11}$ Pa, $E = 10^{11}$ Pa and $E = 2.10^{11}$ Pa and for $\theta = 10^{-6}$, the pressure curves at the upstream end of the pipe are plotted in Figure 17. These two figures indicate that the celerity and the amplitude of the pressure waves decrease by increasing the pipe wall elasticity or by increasing the fluid compressibility. It can be noted that, for example when $\theta = 10^{-6}$, the peak of the pressure wave at the upstream end of the pipe is reduced from 11 MPa when the rigid model is used to 1.8 MPa by using the quasi-rigid model. The transient pressures are satisfactory when simulated by the quasi-rigid model and the finite differences scheme presented herein.

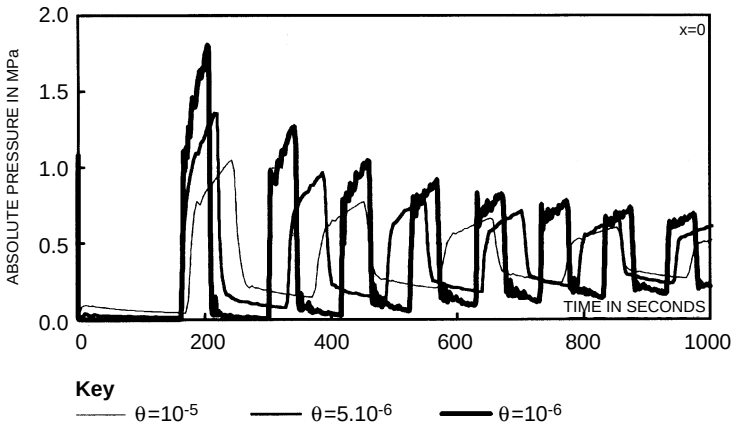

Figure 16.
Computed pressure curves obtained by the quasi-rigid model

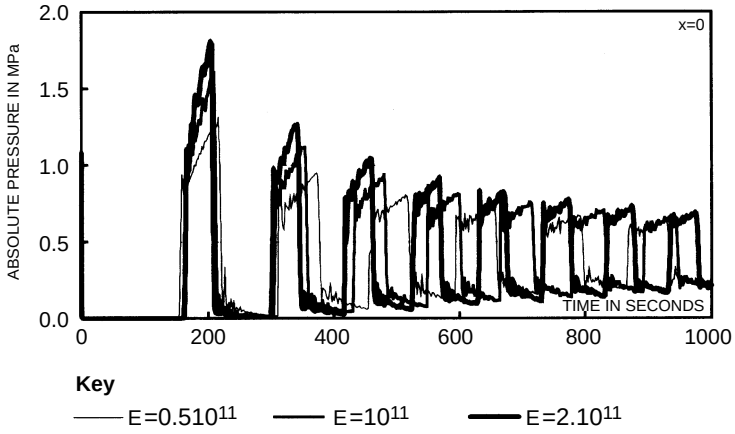

Figure 17.
Computed pressure curves obtained by the quasi-rigid model

For $\theta = 10^{-4}$, Figure 18 shows, the computed pressure evolution obtained in the case of the example one by the rigid and the quasi-rigid models. In this case the two pressure curves are disconcerted. Thus, for relatively great values of θ, the pipe wall elasticity and the liquid compressibility are of minor importance in front of the gas compressibility and the pressure fluctuations are accurately predicted by the simplified rigid model.

6. Conclusion

Two mathematical models have been presented to treat the transient two-phase flows in pipes, the rigid and the quasi-rigid models. They are based on the gas-fluid mass ratio or the quality assumed to be constant. A numerical method has been developed for the computation of the wave pressure propagation following pump failure or valve closure. The rigid model, where the liquid compressibility

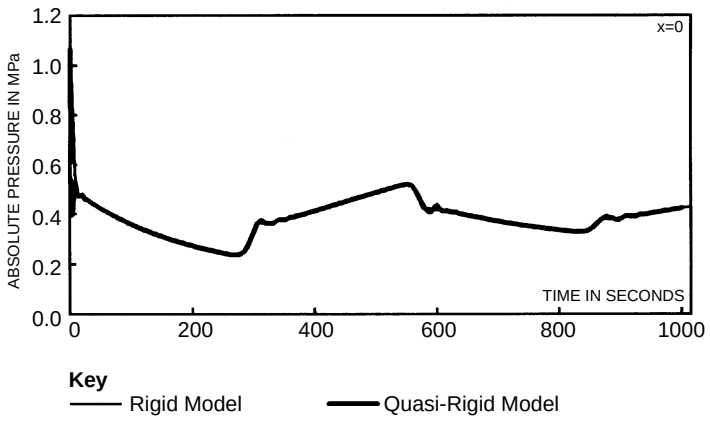

Figure 18. Computed pressure curves obtained for $\theta = 10^{-4}$

and the pipe wall elasticity are neglected may be applied for relatively great values of the quality. For the low values, the pressure amplitudes, computed by the rigid model, with non constant time increment, are very exaggerated and physically unreasonable and in contradiction with the classical water-hammer theory. Including liquid compressibility and pipe wall elasticity in the theory has no great influence in cases where the quality is important. Whereas the influence is considerable in cases where the quality is relatively small or at the limit near to zero. Measured pressure surges subsequent to rapid closure of a downstream valve compare more favourably with numerical results obtained by the quasi-rigid model than by the rigid model. The numerical results obtained by the quasi-rigid model are reasonable and correspond to the reality of the physical problem.

References

1. Campbell, I.J. and Pitcher, A.S., "Shock waves in liquid containing gas bubbles", *Proceeding Royal Society*, London, Vol. 243, 1958, pp. 534-45.
2. Padmanabhan, M. and Martin, C.S. "Shock-wave formation in moving bubbly by steepening of compression waves", *Int. J. Multiphase Flow*, Vol. 4, Pergamon/Elsevier, 1983, pp. 81-8.
3. Martin, C.S. and Padmanabhan, M., "The effect of free gases on pressure transients", *L'Energia Elettrica*, Vol. 5, 1975, pp. 262-67.
4. Martin, C.S., Padmanabhan, M. and Wiggert, D.C., "Pressure wave propagation in two-phase bubbly air-water mixtures", Second International Conference on Pressure Surges, City University, London, England, paper C1, 1-16, 1976.
5. Martin, C.S. and Padmanabhan, M., "Pressure pulse propagation in two-component-slug flow", *Transactions of the ASME, Journal of Fluids Engineering*, Vol. 101, 1979, pp. 44-52.
6. Chaudry, M.H., Bhallamudi, S.M., Martin, C.S. and Naghash, M., "Analysis of transient in bubbly homogeneous, gas-liquid mixtures", *ASME Journal of Fluids Engineering*, Vol. 112, 1990, pp. 225-31.
7. Mori, Y., Hijikata, K. and Komine, A., "Propagation of pressure waves in two-phase flow", *Int. Journal of Multiphase Flow*, Vol. 2, Pergamon/Elsever, 1975, pp. 139-52.

8. Pascal, H., "Compressibility effect in two-phase flow and its application to flow metering with orifice plate and convergent-divergent nozzle", *Transactions of the ASME, Journal of Fluids Engineering*, pp. 105, 1983, 394-99.
9. Evangelesti, G., Boari, M., Guerrini, P. and Rossi, R., "Some application of water-hammer analysis by the method of characteristics", *L'Energia Elettrica*, Vol. 1, 1973, pp. 1-12.
10. Kranenburg, C., "Gas release during transient cavitation in pipes", *Journal of the Hydraulics Division, ASCE 100*, No. HY 10, 1974, pp. 1383-98.
11. Streeter, V.L. and Wylie, E.B., *Hydraulic Transients*, FEB Press, Ann Arbor, MI, 1982.
12. Hadj-Taeb, E. and Khabou, M.T., "Mathematical modelling of transient bubbly cavitating flow in pipelines", *International Conference Computer Application in Water Supply and Distribution*, Leicester, England, Vol. 1, 1993, pp. 123-38.
13. Richtmeyer, R.D. and Morton, K.W., *Difference Methods for Initial Value Problems*, Intersciences Publishers, a division of John Wiley & Sons, New York, NY, 1967.
14. Peyret, R. and Taylor, T.D., *Computational Methods for Fluid Flow*, Springer-Verlag, New York, NY, Heidelberg/Berlin, 1982.
15. Stuckenbruck, S., Wiggert, D.C. and Otwell, R.S., "The influence of pipe motion on acoustic wave propagation", *Transactions of the ASME*, Vol. 107, 1985, pp. 518-22.
16. Stoer, J. and. Buirsch, R., *Introduction to Numerical Analysis*, Springer Verlag, 1983.
17. Wiggert, D.C. and Sundquist, M.J. , "The effect of gaseous cavitation on fluid transients", *ASME Journal of Fluids Engineering*, Vol. 101, 1979, pp. 79-86.
18. Esfandiari, C., "Simulation numérique des écoulements pulsés instationnaires dans les conduites avec singularité de section", *Thèse de Docteur Ingénieur*, ENSAM, Paris, France, Vol. 10, 1985, p. 13.